BRAIN
ORIGINAL ARTICLE

Brain injections of glial cytoplasmic inclusions induce a multiple system atrophy-like pathology

Margaux Teil,[1,†] Sandra Dovero,[1,†] Mathieu Bourdenx,[1,†] Marie-Laure Arotcarena,[1,†] Sandrine Camus,[1] Gregory Porras,[1] Marie-Laure Thiolat,[1] Ines Trigo-Damas,[2,3,4] Celine Perier,[3,5] Cristina Estrada,[6,7] Nuria Garcia-Carrillo,[8] Michele Morari,[9] Wassilios G. Meissner,[1,10] María Trinidad Herrero,[6,7] Miquel Vila,[3,5,11,12] Jose A. Obeso,[2,3,4] Erwan Bezard[1,‡] and Benjamin Dehay[1,‡]

[†,‡]These authors contributed equally to this work.

Synucleinopathies encompass several neurodegenerative diseases, which include Parkinson's disease, dementia with Lewy bodies and multiple system atrophy. These diseases are characterized by the deposit of α-synuclein aggregates in intracellular inclusions in neurons and glial cells. Unlike Parkinson's disease and dementia with Lewy bodies, where aggregates are predominantly neuronal, multiple system atrophy is associated with α-synuclein cytoplasmic inclusions in oligodendrocytes. Glial cytoplasmic inclusions are the pathological hallmark of multiple system atrophy and are associated with neuroinflammation, modest demyelination and, ultimately, neurodegeneration.

To evaluate the possible pathogenic role of glial cytoplasmic inclusions, we inoculated glial cytoplasmic inclusion-containing brain fractions obtained from multiple system atrophy patients into the striatum of non-human primates. After a 2-year *in vivo* phase, extensive histochemical and biochemical analyses were performed on the whole brain.

We found loss of both nigral dopamine neurons and striatal medium spiny neurons, as well as loss of oligodendrocytes in the same regions, which are characteristics of multiple system atrophy. Furthermore, demyelination, neuroinflammation and α-synuclein pathology were also observed. These results show that the α-synuclein species in multiple system atrophy-derived glial cytoplasmic inclusions can induce a pathological process in non-human primates, including nigrostriatal and striatofugal neurodegeneration, oligodendroglial cell loss, synucleinopathy and gliosis.

The present data pave the way for using this experimental model for MSA research and therapeutic development.

1 Université de Bordeaux, CNRS, IMN, UMR 5293, F-33000 Bordeaux, France
2 HM CINAC, HM Puerta del Sur and CIBERNED and CEU-San Pablo University Madrid, E-28938 Mostoles, Spain
3 Center for Networked Biomedical Research on Neurodegenerative Diseases (CIBERNED), Instituto Carlos III, Madrid, Spain
4 CEU, San Pablo University Madrid, E-28938 Mostoles, Spain
5 Neurodegenerative Diseases Research Group, Vall d'Hebron Research Institute (VHIR)-Center for Networked Biomedical Research on Neurodegenerative Diseases (CIBERNED), Barcelona, Spain
6 Clinical and Experimental Neuroscience Unit, School of Medicine, Biomedical Research Institute of Murcia (IMIB), University of Murcia, Campus Mare Nostrum, 30100 Murcia, Spain
7 Institute of Research on Aging (IUIE), School of Medicine, University of Murcia, 30100 Murcia, Spain

Received June 21, 2021. Revised August 05, 2021. Accepted August 31, 2021. Advance access publication March 14, 2022

8 Centro Experimental en Investigaciones Biomédica (CEIB), Universidad de Murcia, Murcia, Spain
9 Department of Neuroscience and Rehabilitation, Section of Pharmacology, University of Ferrara, via Fossato di Mortara 17-19, 44121 Ferrara, Italy
10 Service de Neurologie—Maladies Neurodégénératives, CRMR Atrophie Multisystématisée, CHU Bordeaux, F-33000 Bordeaux, France
11 Department of Biochemistry and Molecular Biology, Autonomous University of Barcelona (UAB), Barcelona, Spain
12 Catalan Institution for Research and Advanced Studies (ICREA), Barcelona, Spain

Correspondence to: Benjamin Dehay
Institute of Neurodegenerative Diseases, Université de Bordeaux, CNRS UMR 5293
Centre Broca Nouvelle-Aquitaine, 146 rue Léo Saignat, 33076 Bordeaux cedex, France
E-mail: benjamin.dehay@u-bordeaux.fr

Correspondence may also be addressed to: Erwan Bezard
E-mail: erwan.bezard@u-bordeaux.fr

Keywords: α-synuclein; multiple system atrophy; non-human primates; neurodegeneration

Abbreviations: α-syn = α-synuclein; DAT = dopamine transporter; DLB = dementia with Lewy bodies; GCI = glial cytoplasmic inclusion; MSA = multiple system atrophy; NHP = non-human primate; SDS = sodium dodecyl sulphate; SNpc = substantia nigra pars compacta

Introduction

Multiple system atrophy (MSA) is a rare, rapidly progressive neurodegenerative disease. It is clinically characterized by parkinsonism, cerebellar impairment, autonomic dysfunction and pyramidal signs in various combinations.[1] Patients with MSA are divided into the cerebellar subtype, MSA-C, where the olivopontocerebellar system is predominantly affected, and the parkinsonian subtype, MSA-P, with predominant involvement of the nigrostriatal system. The overlapping clinical features with Parkinson's disease, particularly at early disease stages, can challenge the differential diagnosis.

MSA belongs to the family of neurodegenerative diseases termed synucleinopathies, along with Parkinson's disease and dementia with Lewy bodies (DLB). The pathological hallmark of synucleinopathies is the formation of α-synuclein (α-syn)-positive inclusions in brain cells. In Parkinson's disease and DLB, these inclusions are primarily localized in neurons and named Lewy bodies. In MSA, these inclusions mostly occur in oligodendrocytes, the myelin-producing cells of the CNS, and are called glial cytoplasmic inclusions (GCI).[2] The neuropathology of MSA includes neuronal and axonal degeneration, mild oligodendroglial loss,[3,4] myelin degeneration,[5] astrogliosis and microgliosis.[6]

Few animal models exist to study MSA pathology.[7] These models mainly rely on the oligodendroglial overexpression of α-syn, thus leaving a need for models that induce (i) pathology by respecting the stoichiometric balance of α-syn expression; and (ii) without imposing an oligodendroglial α-syn expression. Transgenic mouse models have been developed that overexpress human
α-syn under different oligodendrocyte-specific promoters: proteolipid promoter (PLP),[8,9] myelin basic protein (*Mbp*)[10] and 2′,3′-cyclic nucleotide 3′-phosphodiesterase (*Cnp*).[11] More recently, viral-mediated overexpression of α-syn in rats and non-human primates has been proposed for modelling MSA pathology.[12,13] The injection of pathological forms of α-syn obtained from brain homogenates of a diseased animal or human patient has been used to model synucleinopathies across species. To date, the toxic effects of human-derived samples from patients with various synucleinopathies have been assessed mostly for Parkinson's disease, where Lewy bodies-enriched fractions derived from patients have been used to induce a Parkinson's disease-like pathology in both mice and non-human primates (NHPs).[14–16] Until now, only a few studies have aimed at using MSA patient-derived brain homogenates to evaluate the possible pathogenic role of GCIs. While intracerebral injections of MSA patient-derived brain into transgenic α-syn overexpressing mice have yielded pathological outcomes, no pathology was observed when these brain homogenates were injected into wild-type mice.[17,18] Importantly, no such study has yet been conducted in NHPs.[18–21] NHPs present the benefit of being the closest species to humans in terms of their similarities of dopaminergic neuron physiology (i.e. age-dependent accumulation of neuromelanin), cerebral anatomy, glia versus neuron stoichiometry, overall physiology and cognitive and social behaviours,[22–25] as well as sensitivity to small patient-derived aggregates, at odds with rodents.[15] In this pilot study, we extracted MSA-derived GCI fractions, demonstrated their toxicity in an *in vitro* assay, and injected them in both wild-type mice and NHPs. We show that, 2 years after intrastriatal GCI injection, baboon monkeys exhibited marked nigral and striatal neurodegeneration and a loss of oligodendrocytes leading to demyelination and inflammation. Altogether, intracerebral injection of GCI material in NHPs recapitulated key aspects of MSA neuropathology.

Materials and methods

Ethics statement

Experiments were performed following the European Union directive of 22 September 2010 (2010/63/EU) on the protection of animals used for scientific purposes. The Institutional Animal Care and Ethical Committee of Bordeaux University (CE50, France) approved mice experiments under licence number #24246–2020021916287618. The Institutional Animal Care and Ethical Committee of Murcia University (Spain) approved NHP experiments under licence number REGA ES300305440012.

Purification of GCIs from human MSA brains

GCI purification was conducted as previously described in detail for Parkinson's disease Lewy bodies.[14–16,26] The samples were obtained from brains collected in a Brain Donation Program of the Brain Bank 'GIE NeuroCEB' run by a consortium of Patients Associations: ARSEP (Association for Research on Multiple Sclerosis), CSC (Cerebellar Ataxias), France Alzheimer and France Parkinson. The consents were signed by the patients themselves or their next of kin in their name, following French Bioethical Laws. The Brain Bank GIE NeuroCEB (Bioresource Research Impact Factor number BB-0033–00011) has been declared at the Ministry of Higher Education and Research and has received approval to distribute samples (agreement AC-2013–1887). Human putamen was dissected from fresh frozen post-mortem midbrain samples from two patients with MSA-P exhibiting conspicuous striatal GCI pathology on neuropathological examination (mean age at death: 67.5 ± 3.5 years; frozen post-mortem interval: 17 ± 4 h; GIE NeuroCEB BB-0033–00011). Tissue was homogenized in 9 vol (w/v) ice-cold MSE (10 mM MOPS/KOH, pH 7.4, 1 M sucrose, 1 mM EGTA, 1 mM EDTA) with protease inhibitor cocktail (Complete Mini; Boehringer Mannheim) with 12 strokes of a motor-driven glass/Teflon homogenizer. For GCI purification, a sucrose step gradient was prepared by overlaying 2.2 M with 1.4 M and finally with 1.2 M sucrose in volume ratios of 3.5:8:8 (v/v).[27] The homogenate was layered on the gradient and centrifuged at 160 000*g* for 3 h using an SW32.1 rotor (Beckman). Twenty-six fractions of 500 µl were collected from each gradient from the top (fraction 1) to bottom (fraction 26) and analysed for the presence of α-syn aggregates by filter retardation assay, as previously described, with 45 µl of each fraction deposited.[14] GCI-containing fractions from MSA patients were those between fractions 21 and 23 (Fig. 1A). The amount of α-syn in the GCI fractions was quantified using a human α-syn enzyme-linked immunosorbent assay kit (#KHB0061; Invitrogen/Life Technologies). Of the total fractions, the first patient represented around 60% and the second represented around 40%. Quantification by enzyme-linked immunosorbent assay indicated that the GCI mix contained ∼24 pg of α-syn per microlitre. In all cases, samples were bath-sonicated for 5 min before *in vitro* and *in vivo* injections.

Rat ventral midbrain primary cultures

Postnatally derived ventral midbrain cultures were prepared as described.[28] Briefly, cultures were prepared in two steps. In the first step, rat astrocyte monolayers were generated as follows. The entire cerebral cortex from a single rat pup (postnatal Days 1–2) was removed, diced and then mechanically dissociated by gentle trituration. The isolated cells were plated at a concentration of 80 000 cells onto wells under which a laminin-coated coverslip was affixed. The cells were housed at 37°C in an incubator in 5% CO_2 and were fed on glial media. Once confluence had been attained, fluorodeoxyuridine (6.7 mg/ml) and uridine (16.5 mg/ml) were added to prevent additional proliferation. In the second step, rat pups aged between 1 and 2 days were anaesthetized, and 1-mm^3 blocks containing ventral midbrain neurons were dissected from 1-mm thick sagittal sections taken along the midline of the brain. Tissues were collected immediately into cold phosphate buffer and were treated enzymatically using papain (20 U/ml) with kynurenate (500 µM) at 37°C under continuous oxygenation with gentle agitation for 2 h. A dissociated cell suspension was achieved by gentle trituration and was then plated onto the pre-established glia wells at a density of 0.5–1.7 million neurons per well. Cultures were maintained in specially designed neuronal media containing 27 µM fluorodeoxyuridine and 68 µM uridine to control glial outgrowth and in 10 ng/ml glial cell-derived neurotrophic factor. They were incubated for a further 7–8 days before GCI-derived exposure. Primary culture dopaminergic cells were exposed to 1 µl of GCI fractions for 24 h. Then, primary cultures were fixed in 4% paraformaldehyde, blocked and incubated with a primary rabbit anti-TH (1:1000, Calbiochem, Cat#657012) and corresponding fluorescence-conjugated secondary antibodies. All TH-positive neurons were analysed by fluorescence microscopy and counted on each plate.

Animals and stereotactic injections

Mice

Wild-type C57BL/6J mice (3 months old) received 2 µl of either GCI fractions ($n = 10$) or sucrose ($n = 5$) by stereotactic delivery to the region immediately above the right substantia nigra, to avoid mechanical lesion and to cover the whole substantia nigra (coordinates from Bregma: AP = –2.9, L = +1.3, DV = –4.5) at a flow rate of 0.4 µl/min and the pipette was left in place for 5 min after injection to avoid leakage as previously described.[14,15,26,29] Mice were perfused 4 months after injection using 0.9% NaCl followed by 4% paraformaldehyde. Brains were then post-fixed for 24 h in 4% paraformaldehyde at 4°C, cryoprotected in gradient 20% sucrose in phosphate-buffered saline (PBS) before being frozen by immersion in a cold isopentane bath (–60°C) and stored immediately at –80°C until sectioning for histochemical analysis.

Non-human primates

Experiments were conducted as previously described[15,16] at the research animal facility of the University of Murcia (Murcia, Spain). Adult female and male olive baboons ($n = 8$; *Papio papio*) ranging from 3 to 14 years of age were housed in two multi-male multi-female exterior pens. Animals were fed fruits, vegetables and dry food pellets twice a day before 9 a.m. and after 5 p.m. Water was available *ad libitum*. Allocation to experimental groups was randomized. Three baboons were used for GCI injections and five were untreated control animals. Intrastriatal injections of GCI fractions were performed at two rostrocaudal levels of the motor striatum (anterior commissure, –1 mm and –5 mm) under stereotactic guidance as previously described.[15,16] The total injected volume per hemisphere was 100 µl (2 injection sites with 50 µl each at 3 µl/min at each location site). After each injection, the syringe was left in place for 10 min to prevent leakage along the needle track. Several parameters were monitored during the 2-year study, including survival and clinical observations. At the end of the experiment, all baboons were terminated with pentobarbital overdose (150 mg/kg i.v.), followed by perfusion with room-temperature 0.9% saline solution (containing 1% heparin) following accepted European Veterinary Medical Association guidelines. Brains were removed quickly after death. Each brain was then dissected along the midline and each hemisphere was divided into three parts. The left hemisphere was immediately frozen by immersion in a cold isopentane bath at –50°C for at least 5 min and stored at –80°C for biochemistry investigations. The right hemisphere was post-fixed 1 week in 10 vol/tissue of 4% paraformaldehyde at 4°C, cryoprotected in two successive gradients of 20% then 30% sucrose in PBS before being frozen by immersion in a cold isopentane bath (–50°C) during at least 5 min and stored immediately at –80°C until sectioning. No sample was excluded from analysis in these studies.

Non-human primate behavioural assessment

Following a 4-h habituation phase performed one day before the beginning of the observations, baboon behaviour was observed outside the feeding and cleaning times, in random order at two

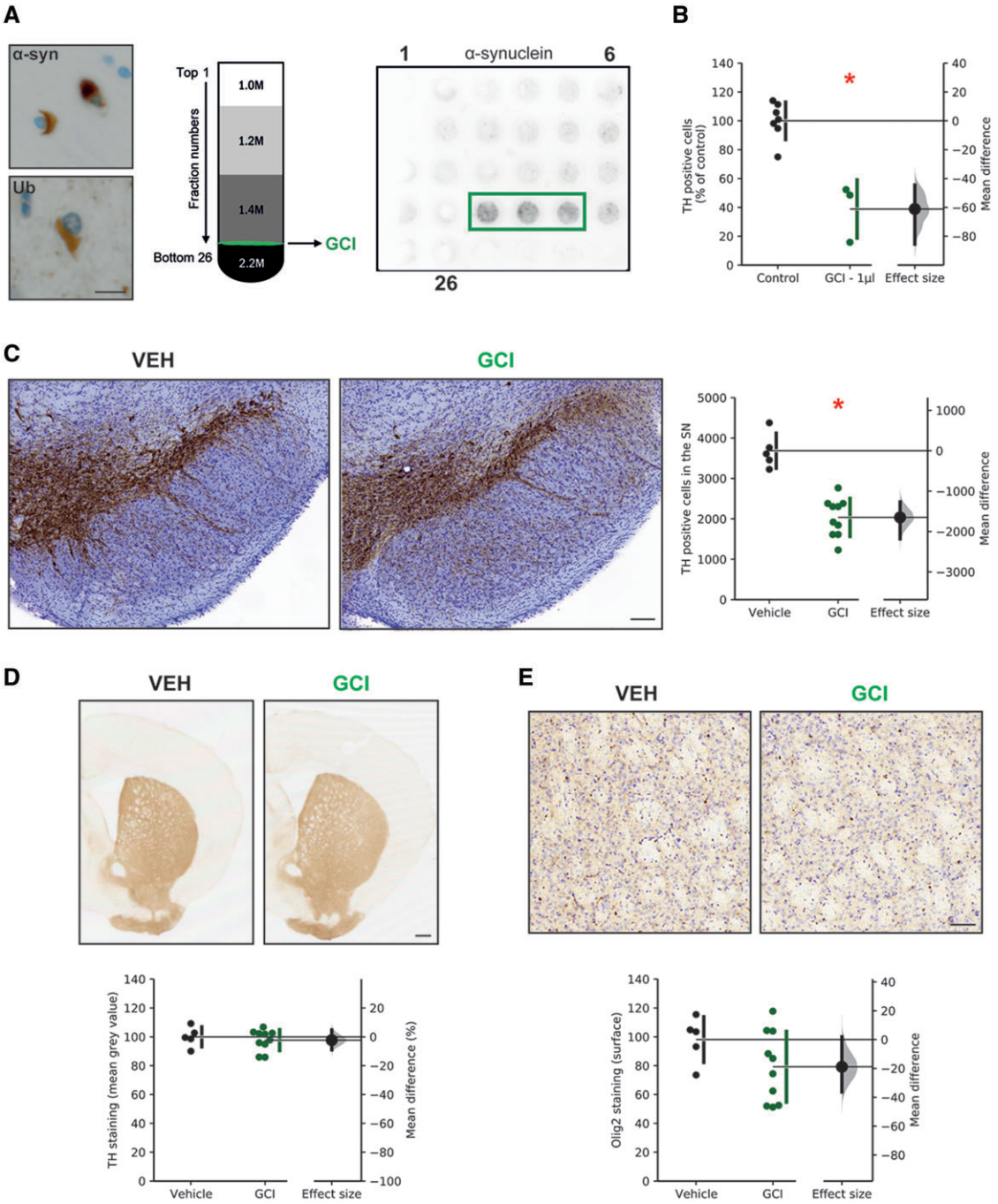

Figure 1 Purified GCI from MSA patient brains induce neurodegeneration in mice. (**A**) *Left*: α-Syn and ubiquitin (Ub) immunohistochemistry of striatal post-mortem brain samples unravelling GCIs. Scale bar = 200 µm. *Middle*: Schematic representation of the sucrose gradient fractionation procedure used to purify GCI-containing fractions from freshly frozen post-mortem nigral brain tissue of two MSA-P patients. *Right*: Filter retardation assay probed with a human specific α-syn antibody to assess the presence of insoluble α-syn aggregates in the different fractions obtained by sucrose gradient fractionation from freshly frozen post-mortem striatal brain tissue of MSA patients. The green rectangle indicates the GCI-containing fractions selected to prepare the mixture used for GCI injections. (**B**) Scatter plots of tyrosine hydroxylase (TH) immunopositive rat mesencephalic cells treated with 1 µl of GCI fractions for 24 h and expressed as a percentage of controls; $P = 0.0002$, $t = 5.872$. (**C**) Illustrative image (*left*) and quantification (*right*) of TH immunopositive cells by stereological counting in the substantia nigra pars compacta (SNpc) of GCI-injected and control mice; $P < 0.0001$, $t = 6.581$. Scale bar = 100 µm. (**D**) Illustrative image (*top*) and quantification (*bottom*) of TH immunostaining measured by optical density in the striatum of GCI-injected and control mice, normalized by controls; $P = 0.2818$, $t = 0.5926$. Scale bar = 500 µm. (**E**) Illustrative image (*top*) and quantification (*bottom*) of Olig2 immunostaining in the striatum of control and GCI-injected mice expressed as surface threshold occupied by Olig2 normalized by controls; $P = 0.0720$, $t = 1.555$. Scale bar = 50 µm. The horizontal line indicates the average value per group ± standard deviation (SD). Each dot represents one mouse of the control (black) and GCI-injected group (green). Bootstrapped mean difference with 95% CI (error bar) is shown on the right side of each graph. Comparisons were made using an unpaired *t*-test. *$P < 0.05$ compared to control animals. VEH = vehicle.

time points (morning and afternoon) over 4–9 days (eight sessions per group) as previously described.[15] On the first observational time point (i.e. 1-month post-surgery), the habituation phase was performed over 3 days, allowing the observer to recognize the animals individually. We used a scan-sampling method, appropriate for time budgeting, in which behavioural parameters were assessed every 5 min during 2-h sessions, resulting in 192 scans per individual.[30–32] A unique trained observer blind to the experimental conditions (S.C.; intra-observer reliability: Spearman rank-order correlation $R = 0.987$) collected the data live at the study's two time points: 1 and 24 months post-surgery. The observer stood 1 m away from the outdoor cages and focused on behavioural profiles rather than single items. Two repertoires were used: one reports the interaction with the environment and one describes the position within the environment, according to published protocols and data collection by the very same observer.[30–32] We investigated the percentages of each item's occurrence about the total number of scans to obtain mean behavioural and postural time budgets, body orientation and location profiles.

Histological analysis

Neurodegeneration

To assess the effect of GCI injections in both mice and monkeys on dopaminergic neurons and fibres, TH, AADC (aromatic L-amino acid decarboxylase) and DAT (dopamine transporter) immunohistochemistry were performed on striatal and/or SNpc sections as previously described.[15,16] For TH staining sections were selected in the posterior striatum and serial sections (1–12 for monkeys and 1–6 for mice) of whole SNpc, AADC and DAT in the medial striatum at the level of the anterior commissure. Sections were incubated with rabbit monoclonal TH antibody (Millipore, MAB318, 1:5000), rabbit polyclonal AADC antibody (Merck AB136, 1:1000) or rat monoclonal DAT antibody (Merck MAB369, 1:1000) for one night at room temperature and revealed the next day with the corresponding peroxidase EnVision secondary antibody, followed by 3,3′-diaminobenzidine (DAB) visualization. SNpc sections were mounted on gelatin-coated slides, counterstained with 0.1% cresyl violet solution, dehydrated and cover-slipped. Striatal sections were mounted on gelatin-coated slides, dehydrated and cover-slipped. Striatal sections were analysed by optical density in the caudate nucleus and putamen. The slides were scanned using Epson expression 10000XL high-resolution scanner and images were analysed using ImageJ open-source software (version 1.53) to compare mean grey levels in the caudate nucleus and putamen. TH-positive neurons of the SNpc were counted by stereology blind about the experimental condition using a Leica DM6000B microscope coupled with the Mercator software (Explora Nova, France). The SNpc was delineated for each slide, and probes for stereological counting were applied to the map obtained. Each TH-positive cell with the neuron included in the probe was counted. The total number of TH-positive neurons in the SNpc per hemisphere was then assessed using the optical fractionator method.

Oligodendroglial loss

Olig2 (oligodendrocyte transcription factor 2) and myelin immunohistochemistry were performed as previously described with minor changes[12] to assess oligodendroglial loss in the striatum of mice and monkeys. Sections were selected in the medial to posterior striatum and were incubated with mouse monoclonal Olig2 antibody (Merck, MABN5044, 1:1000) or rabbit monoclonal myelin basic protein antibody (Abcam, ab218011, 1:5000) for one night at room temperature and revealed the next day by an anti-mouse or anti-rabbit peroxidase EnVision secondary antibody, respectively, followed by DAB visualization. Free-floating Olig2-stained sections were mounted on gelatin slides, counterstained with 0.1% cresyl violet solution, dehydrated and cover-slipped. Free-floating myelin-stained sections were mounted on gelatin slides, dehydrated and cover-slipped. Slides were scanned using the Panoramic Scanner and analysed using the Mercator software (Explora Nova, France). Olig2 slides were analysed using a surface threshold, where the baseline detection signal was determined and then applied on all slides. Myelin slides were analysed in two ways: using surface threshold similarly to Olig2 staining and using optical density measuring the mean grey staining in the white matter in striatal sections. In addition, we measured the Nissl-cell count in the putamen on Olig2-counterstained sections using stereology.

Synuclein staining

Pathological handling of synuclein was assessed in monkeys with a mouse monoclonal antibody raised against human α-syn (syn211, ThermoFisher, MA5-12272, 1:1000) and another against phosphorylated α-syn (clone11A5, Elan, 1:5000), as previously reported.[14,15] Briefly, selected sections at two rostrocaudal levels were specifically identified and incubated in the same well to allow direct comparison of immunostaining intensity. Sections were incubated overnight at room temperature with the aforementioned antibodies. The following day, the revelation was performed with anti-species peroxidase EnVision system (Dako) followed by DAB incubation. Sections were then mounted on gelatinized slides, dehydrated, counterstained if necessary and cover-slipped until further analysis. Grey-level quantification or immunostaining-positive surface quantification in 29 brain regions were performed as previously described.[15,16] A heat map was generated using the data from grey-level quantifications in the different brain regions.[33]

Second, to assess the accumulation of total α-syn in cells in the SNpc, staining was performed on serial sections (1–12) of SNpc, corresponding to the whole SNpc.[16] Sections were incubated in monoclonal mouse Syn211 antibody for one night at room temperature and revealed the next day using an anti-mouse peroxidase EnVision secondary antibody followed by DAB visualization. Syn211-positive cells were counted using the Mercator software (Explora Nova, France). The SNpc was delineated for each slide, and probes for stereological counting were applied to the map obtained. Each Syn211-positive cell with the nucleus included in the probe was counted. The total number of Syn211-positive neurons in the SNpc was then assessed using the optical fractionator method.

Inflammation

Inflammatory processes in striatal sections were measured as previously described[15,16] through GFAP/S-100 (Dako, Z0334/Abnova, PAP11341) and Iba1 (Abcam, ab5076) immunohistochemistry. Striatal sections were incubated overnight with a mix of rabbit antibodies raised against GFAP and S-100 for the astroglial staining (respective dilutions 1:2000 and 1:1000), and with a goat anti-Iba1 antibody for the microglial staining (dilution 1:1000). These signals were revealed with anti-species peroxidase EnVision system (Dako) followed by DAB incubation. GFAP-S100 sections were mounted on slides, counterstained in 0.1% cresyl violet solution, dehydrated and cover-slipped. Sections stained by Iba1 were mounted on slides, dehydrated and cover-slipped. Sections stained by GFAP-S-100 were numerized at ×20 magnification with a NanoZoomer (Hamamatsu) and Iba1 sections were numerized using the Panoramic Scanner. All quantifications were estimated by immunostaining-positive surface quantification at regional levels with the Mercator software (Explora Nova, France).

Biochemical analysis in non-human primates

Total protein extraction

Tissue patches collected on 300-µm thick cryostat-cut sections of caudate nucleus and putamen ($n = 5$ patches per structure and animal) were extracted on ice using 100 µl of RIPA buffer [50 mM tris-HCl (pH 7.4), 150 mM NaCl, 1.0% Triton X-100, 0.5% Na-deoxycholate, and 0.1% SDS] with a protease and phosphatase inhibitor cocktail as previously described.[15,16] Lysates were incubated for 20 min and then centrifuged at 14 000 rpm for 15 min at 4°C. Supernatants were collected, and the total amount of protein in the lysates was assessed by bicinchoninic acid assay before storage at –80°C.

Based on total protein concentrations from the bicinchoninic acid assays, aliquots of tissue lysates corresponding to known amounts of total protein per sample were prepared for each animal in Laemmli buffer (Tris-HCl 25 mM pH 6.8, glycerol 7.5%, SDS 1%, DTT 250 mM, and bromophenol blue 0.05%) for immunoblotting experiments.

Sequential protein extraction

Tissue patches, collected as above ($n = 10$ patches per structure and per animal) were homogenized in Triton-X extraction buffer (50 mM Tris-base pH 7.6, 150 mM NaCl, 1% Triton-X-100, 2 mM EDTA) containing protease and phosphatase inhibitors as previously described.[15,16,34] The lysate was sonicated and then centrifuged (120 000*g* for 60 min at 4°C) and the supernatant was collected (Triton-X-soluble fraction). The pellet was then washed three times with 1 M PBS/1% Triton-X, centrifuged (13 000*g* for 15 min) and resuspended in SDS extraction buffer (50 mM Tris pH 7.6, 150 mM NaCl, 1% Triton-X-100, 0.5% Na-deoxycholate, 1% SDS), sonicated and centrifuged (120 000*g* for 60 min at 4°C) and the supernatant was collected (Triton-X-insoluble fraction).

Immunoblotting

Western blots were run in all conditions using 20 µg of protein separated by SDS–polyacrylamide gel eletrophoresis and transferred to nitrocellulose membranes, as previously described.[15,16] Incubation of the primary antibodies was performed overnight at 4°C with rabbit anti-phosphorylated-α-syn at Ser129 (1:5000, Abcam EP1536Y), Syn1 (1:1000, BD Biosciences), Syn211 (1:1000, ThermoFisher), TPPP/p25a (1:5000, Sigma). Anti-β-actin (1:2000, Sigma) was used to control equal loading. Appropriate secondary antibodies coupled to peroxidase were revealed using a Super Signal West Chemiluminescent kit (Immobilon Western, Chemiluminescent HRP substrate, Millipore). Chemiluminescence images were acquired using the ChemiDoc + XRS system measurement (Bio-Rad). Signals per lane were quantified using ImageJ (version 1.53). A ratio (protein of interest normalized to β-actin protein levels, then to Control values) of the signal on loading per animal was performed and used in statistical analyses.

Neurotransmitter analysis in non-human primates

Tissue patches collected on 300-µm thick cryostat-cut sections of globus pallidus pars internalis ($n = 5$ patches per structure and animal) were prepared and analysed as previously described,[15] homogenized in methanol/water (50:50% v/v), then centrifuged at 14 000 rpm for 15 min at 4°C.[35] The supernatant was aliquoted and stored at –80°C until amino acid derivatization. Glutamate and GABA content in the samples was measured by high-performance liquid chromatography coupled with fluorometric detection (FP-2020 Plus fluorimeter, Jasco) after precolumn derivatization with o-phthaldialdehyde (OPA)/mercaptoethanol reagent.[36] Thirty microlitres of OPA reagent were automatically added to a 28-µl sample by a refrigerated autosampler kept at 4°C (Triathlon, Spark Holland). Fifty microlitres of the mixture were injected onto a 5-C18 Hypersil ODS column (3 × 100 mm; Thermo-Fisher) perfused at 0.48 ml/min (Jasco PU-2089 Plus Quaternary Pump) with a mobile phase containing 0.1 M sodium acetate, 10% methanol, 2.2% tetrahydrofuran (pH 6.5). Chromatograms were acquired and analysed using ChromNav software (Jasco, Tokyo, Japan). Under these conditions, the limits of detection for glutamate and GABA were ∼1 nM and ∼0.5 nM, and their retention times ∼3.5 min and ∼18.0 min, respectively.

Immunofluorescent labelling in non-human primates

Double-immunofluorescent labelling was performed on striatal sections to localize the accumulation of α-syn. Sections were permeabilized and blocked using normal donkey serum or normal goat serum diluted in PBS 1×-Saponine 0.2% for 1 h before being incubated overnight in primary antibodies [mouse anti-CNPase (1:1000, ab237961, Abcam) or mouse anti-NeuN (1:1000, MAB377, Merck) and rabbit anti-α-syn (1:5000, MJFR1, ab209420, Abcam) or rabbit anti-phosphorylated α-syn at Ser129 (1:2000, EP1536Y, ab51253, Abcam)]. The next day, sections were incubated in secondary antibodies sequentially: first with donkey anti-mouse Alexa 488 secondary antibodies, then with donkey anti-rabbit Alexa 568 (α-syn) or Alexa 647 (pSyn) secondary antibodies. After washing, sections were incubated with 10 µM of Hoechst staining for 8 min to colour the nuclei. Sections were mounted on non-gelatinized slides and cover-slipped using fluorescent mounting media without DAPI (Vector Labs). Images were acquired using a Zeiss SP5 confocal microscope (×63). Analysis of images was done using ImageJ (version 1.53), with a macro designed to delineate individual cells, analyse particles within the cell and extrapolate the count and size of puncta.

Statistical analysis

Principal component analysis was performed in Python (Python software foundation v.3.7.4 available at https://www.python.org/) and the scientific python stack: scipy (v.1.4.1),[37] numpy (v.1.18.1),[38] matplotlib (v.3.3.3)[39] and scikit-learn (v.0.22.1).

For all experiments, comparisons among means were performed using raw data by using Student's one-tailed unpaired t-test (GraphPad Prism 9.0, San Diego, CA). Correlations between variables were assessed with Spearman's correlation analysis. Statistical significance was set at $P < 0.05$.

The debate about the need to move beyond *P*-value is raging. Data must now be analysed further with estimation graphics[40] that put the emphasis on the effect size. Therefore, all data appear as estimation graphics called 'Gardner–Altman plots': on the left of each graph, data of vehicle (mice) or controls (NHP) and GCI groups are presented as scatter plots showing the observed values along with above-defined descriptive statistics (mean ± SD). On the right of each graph, a contrast graph using the difference axis to display an effect size, here mean difference. Horizontally aligned with the mean of the test group, the mean difference is indicated by the black circle. The 95% CI of the mean difference is illustrated by the black vertical line. The grey curve indicates the resampled distribution of the effect size, given the observed data.

Data availability

The data supporting the findings of this study are available from the corresponding authors upon reasonable request.

Results

Qualification of GCI-containing fractions from human MSA brains

GCI-enriched fractions were obtained from two MSA patient brains, containing conspicuous α-syn-positive and ubiquitin-positive aggregates (Fig. 1A). They were used to evaluate the pathological consequences of injecting α-syn-containing putaminal GCI extracts purified from MSA-P patients into the brains of wild-type mice and NHPs. Fresh-frozen post-mortem striatal samples were purified through differential ultracentrifugation using a sucrose step gradient and tested for their α-syn immunoreactivity using filter retardation assay (Fig. 1A), as previously described.[14–16]

GCI fractions were first tested *in vitro* on rat mesencephalic primary cultures. GCI fraction administration induced a significant loss of TH-positive cells by over 50% (Fig. 1B), thereby demonstrating the toxicity of GCI fractions. This raised the question of whether these fractions also have harmful effects *in vivo*. To test this, wild-type mice received intranigral injections of GCI fractions. Four months after administration, mice presented a significant 39±4.5% loss of dopaminergic neurons in the substantia nigra (Fig. 1C), without losing dopaminergic fibres projecting to the striatum (mean difference lower than 5%; Fig. 1D). Possibly owing to the relatively short live phase, no significant loss of striatal oligodendrocytes was observed, although a trend towards a decrease was noticeable with an effect size of ∼20% in Olig2 staining (Fig. 1E). Overall, these results confirmed the toxicity of putaminal-derived GCI fractions extracted from MSA patients onto substantia nigra cells in wild-type mice and grounded the NHP experiment.

GCIs-containing fractions induce nigral and striatal degeneration in non-human primates

Following our *in vitro* and *in vivo* mice experiments, we aimed to determine whether GCI fractions affected NHPs. GCI-injected baboons were ethologically followed for 2 years after administration. We observed motor difficulties with an increase in the time spent with their body oriented in the open environment, indicating anxiety-like behaviour and decreased time spent in the corridor connecting the main aviary to the secondary, indicating decreased motivation/locomotion[31] (Supplementary Fig. 1A and B). These subtle phenotypes are reminiscent of those displayed by Lewy body-injected monkeys[15] and suggest that GCI-injected monkeys might have been in a prodromal phase. Post-mortem examination 2 years after injection unravelled that GCI injection induced a significant impairment of the nigrostriatal pathway with TH immunoreactivity losses of 36% in the caudate nucleus (Fig. 2A–D), 18% in the putamen (Fig. 2A and E) and 40% in the substantia nigra (Fig. 2A, F and G). AADC, the enzyme that decarboxylates L-DOPA into dopamine (Fig. 2H) and striatal DAT immunostaining were also reduced (Fig. 2I) with a mean difference between groups of ∼50% for both markers in caudate and putamen. GCI-injected monkeys also presented a significant decrease of the density of Nissl-positive cells in the putamen (Fig. 2J), suggesting a loss of striatal medium spiny neurons. Together, these results reflect an impairment and degeneration of the nigrostriatal pathway and putamen.

Next, we performed dimensionality reduction using principal components analysis (a multivariate analysis method). Projection of individual points along PC1–PC2 demonstrated that neurodegeneration-related variables allowed clustering of controls and GCI-injected animals in two opposite parts of the PC1–PC2 space with no overlap (Fig. 2K). Most of the variance was captured by PC1 (70.3%), which showed high correlation values with most neurodegeneration-related variables (Supplementary Table 1 features all raw data). Analysis of individual scores along the PC1 axis showed significant differences between controls and GCI-injected animals (Fig. 2L). Altogether, these results confirmed the harmful impact of GCI fractions on the nigro-striatal pathway integrity in monkeys.

Because both the substantia nigra and the striatum exhibited neurodegeneration, we wondered whether these changes resulted into functional changes into the basal ganglia network. Glutamate levels slightly increased (∼20%) while GABA content decreased in GCI-injected monkeys (Supplementary Fig. 2A and B). This is consistent with (i) an increased activity of the glutamatergic projection from subthalamic nucleus, i.e. the last relay nucleus of the indirect pathway; and (ii) a decreased drive from the GABAergic projection that composes the direct pathway.[41] Both changes sign an imbalance of striatofugal pathways, resulting from neurodegeneration.

GCIs-containing fractions induce oligodendrocyte loss in non-human primates

Given that MSA pathology is not only characterized by the loss of striatal and dopaminergic neurons but also by oligodendrocyte dysfunction and consequently myelin disruption, we evaluated whether this could be observed at the striatal and white matter levels in GCI-injected monkeys. Histochemical analysis of Olig2 staining showed a significant decrease in the caudate nucleus and the putamen, in terms of both total surface and cell size (Fig. 3A–F). No significant changes, but trends, due to the small sample size, were observed in the white matter, with a mean difference in Olig2 staining of 60% (Fig. 3G–I). Our results suggested a decrease in the total number and the size of striatal oligodendrocytes in GCI-injected monkeys. We next examined the myelination, one of the crucial roles of oligodendrocytes, using myelin immunostaining in the putamen of GCI-injected and control animals. We observed a decrease in myelin immunoreactivity in the white matter of GCI-injected monkeys (Fig. 3J–L).

Interestingly, the loss of putaminal oligodendrocytes correlated positively with the loss of striatal dopamine fibres, DAT and AADC staining (Supplementary Fig. 3A and B) and striatal cell density (Supplementary Fig. 3C). Moreover, the oligodendroglial loss in the white matter also significantly and positively correlated with dopaminergic degeneration (i.e. loss of TH and DAT-positive fibres in the putamen and caudate nucleus; Supplementary Fig. 3D–G). These associations suggested the existence of striatal neurodegeneration affecting both the incoming dopamine fibres and the striatofugal neurons concomitant with oligodendroglial neurodegeneration, thereby corroborating neurochemistry findings.

In MSA, TPPP/p25α is relocated from myelin sheaths to oligodendrocyte cytoplasm and is a significant component of GCIs.[1,5,42,43] We characterized variations in TPPP/p25α protein levels in the putamen and caudate of GCI-injected monkeys, particularly in the putamen with an increase of 25% (Fig. 3M and N).

In addition to oligodendrogliopathy, increased inflammation via astrogliosis and microgliosis has been observed in human MSA neuropathology.[44] We observed that they did not present a marked inflammatory response as indicated by the absence of astrocytic reaction, using the marker GFAP, and microglial proliferation, using Iba1, in the striatum and the white matter (Supplementary Fig. 4A and B). While GFAP staining also remained unaffected in the entorhinal cortex, we observed local increase of microglial surface staining in the entorhinal cortex of GCI-injected monkeys (Supplementary Fig. 4A and B). Altogether these results suggested that, in addition to the mesencephalic and striatal degeneration,

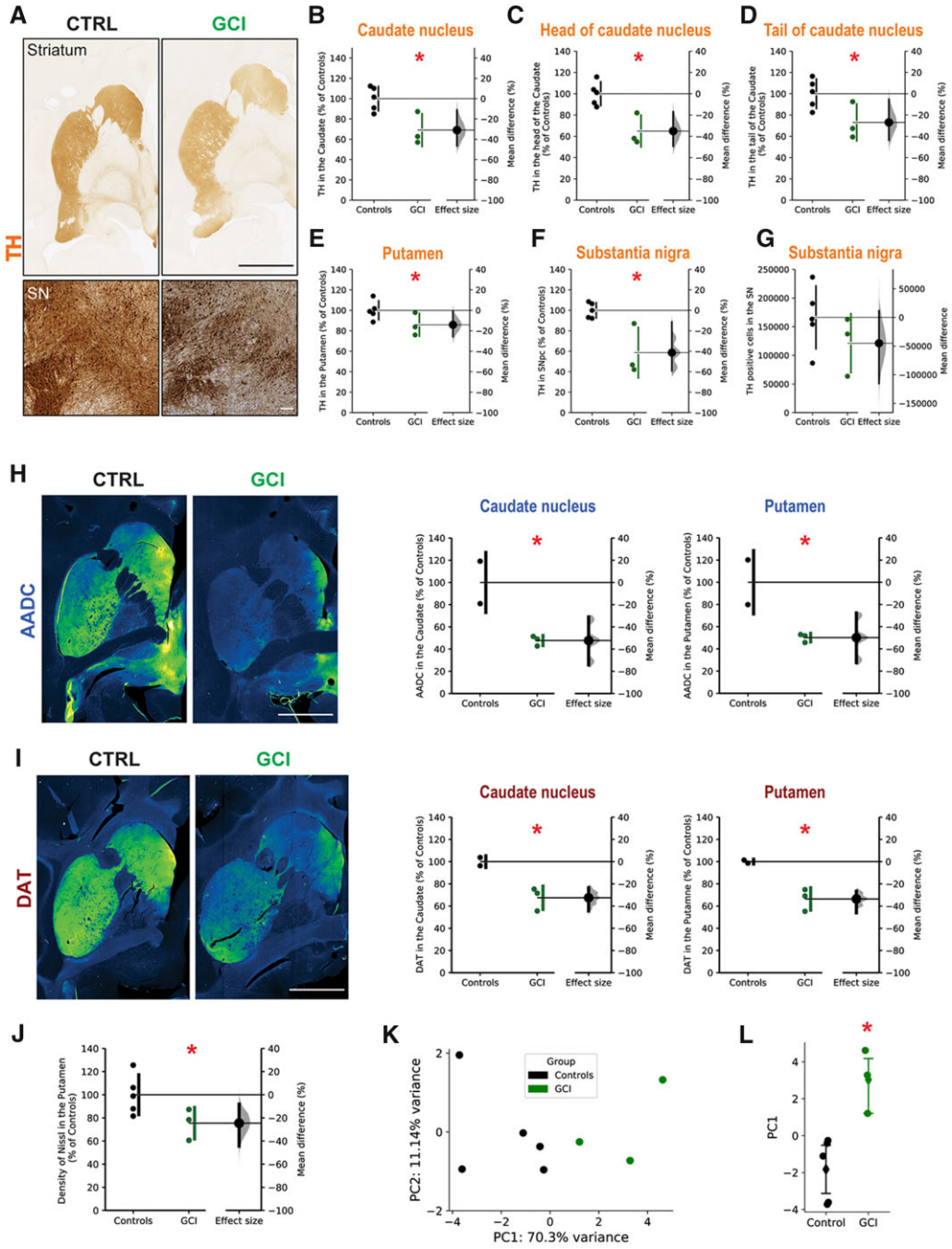

Figure 2 Intrastriatal injection of GCI-derived fractions induces nigrostriatal neurodegeneration in the NHP brain. (**A**) TH immunostaining at striatum and SNpc levels in control ($n = 5$) and GCI-injected baboon monkeys ($n = 3$). Scale bars = 5 mm (striatum) and 200 μm (SNpc). (**B–E**) Scatter plots of mean grey TH immunostaining in the caudate nucleus; $P = 0.0098$, $t = 3.159$ (**B**), in the head of the caudate nucleus; $P = 0.0042$, $t = 3.849$ (**C**), in the tail of the caudate nucleus; $P = 0.0248$, $t = 2.452$ (**D**) and in the putamen; $P = 0.0488$, $t = 1.961$ (**E**) in Control versus GCI-injected baboon monkeys, expressed as a percentage of controls. (**F** and **G**) Scatter plots of TH staining in the substantia nigra by quantification of surface staining, expressed as a percentage of controls; $P = 0.0054$, $t = 3.648$ (**F**) and the number of TH-positive cells; $P = 0.1475$, $t = 1.147$ (**G**). (**H**) Illustrative images (*left*) and scatter plots (*right*) of AADC immunostaining measured by optical density in the caudate nucleus; $P = 0.0187$, $t = 3.573$ and in the putamen; $P = 0.0236$, $t = 3.259$ of control and GCI-injected NHPs and expressed as a percentage of controls. A green fire blue LUT (lookup table) was used to enhance contrast and highlight the difference. Scale bar = 5 mm. (**I**) Illustrative images (*left*) and scatter plots (*right*) of DAT immunostaining measured by optical density in the caudate nucleus; $P = 0.0147$, $t = 3.929$ and in the putamen; $P = 0.0105$, $t = 4.456$ of control and GCI-injected NHPs and expressed as a percentage of controls. A green fire blue LUT was used to enhance contrast and highlight the difference. Scale bar = 5 mm. (**J**) Scatter plot representing the density of Nissl-positive cells in the putamen of control and GCI-injected NHPs, expressed as a percentage of controls. $P = 0.0405$, $t = 2.095$. The horizontal line indicates the average value per group ± SD. Each dot represents one NHP of the control (black) and GCI-injected baboon monkeys (green). Bootstrapped mean difference with 95% CI (error bar) is shown on the *right* side of each graph. Comparisons were made using an unpaired *t*-test. *$P < 0.05$ compared to control animals. (**K** and **L**) Principal component (PC) analysis was applied on 11 neurodegenerative parameters (above). Each animal is represented by a dot in the new space created by PC1–2 (**K**). Histogram plot depicts mean values of PC1 scores for each experimental group; $P = 0.0160$ (**L**). Each dot represents one NHP of the control (black) and GCI-injected baboon monkeys (green).

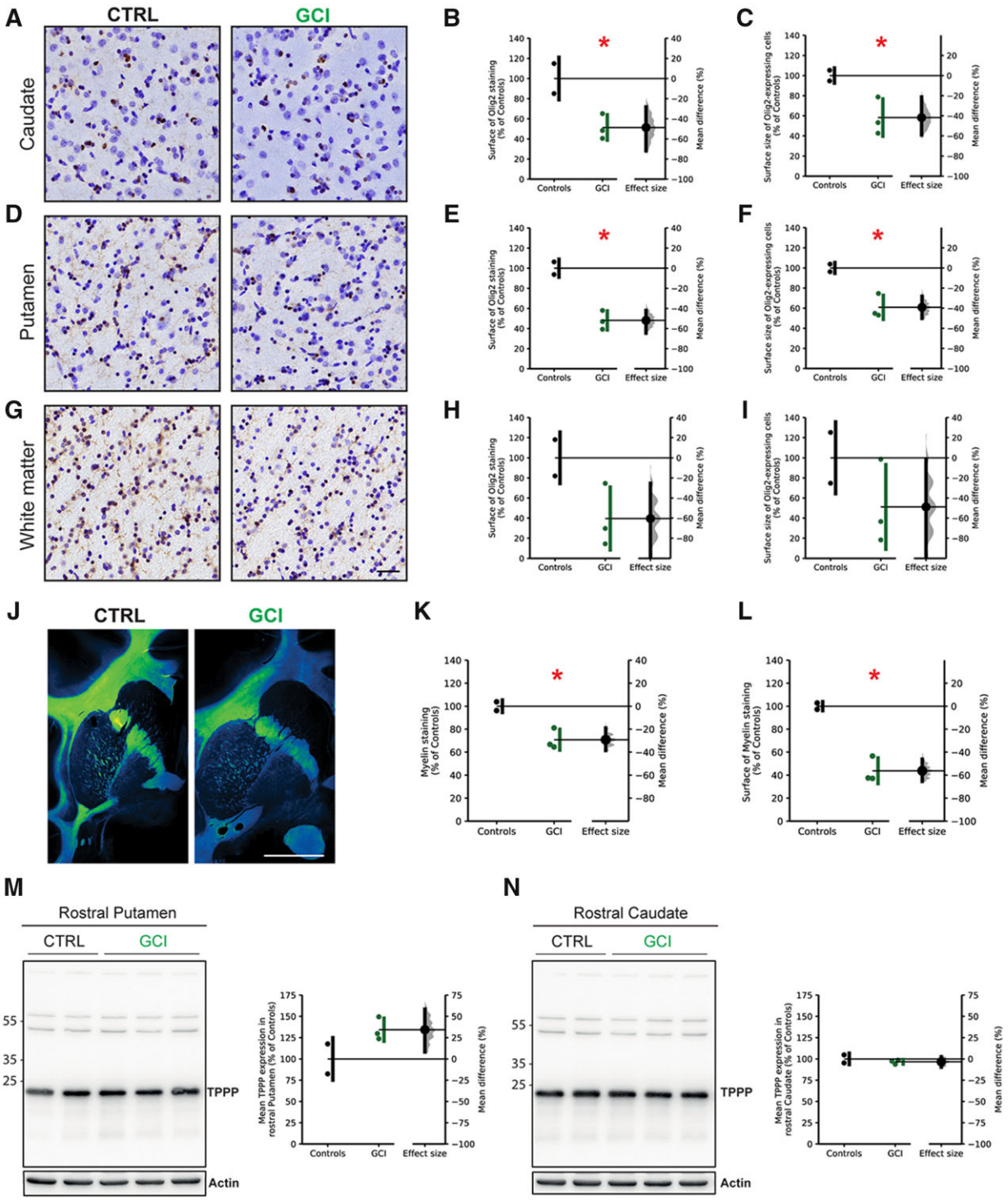

Figure 3 Intrastriatal injection of GCI-derived fractions induces oligodendroglial loss and demyelination in the NHP brain. (**A–C**) Illustrative images (**A**) and quantification (**B** and **C**) of Olig2 immunostaining measured by surface threshold; $P = 0.0221$, $t = 3.346$ (**B**) or surface size; $P = 0.0310$, $t = 0.2911$ (**C**) expressed as a percentage of controls, in the caudate nucleus of control and GCI-injected NHPs. Scale bar = 40 μm. (**D–F**) Illustrative images (**D**) and quantification (**E** and **F**) of Olig2 immunostaining measured by surface threshold; $P = 0.0043$, $t = 6.154$ (**E**) or surface size; $P = 0.0124$, $t = 4.190$ (**F**), expressed as a percentage of controls, in the putamen of control and GCI-injected NHPs. Scale bar = 40 μm. (**G–I**) Illustrative images (**G**) and quantification (**H** and **I**) of Olig2 immunostaining measured by surface threshold; $P = 0.0552$, $t = 2.245$ (**H**) or surface size; $P = 0.1370$, $t = 1.336$ (**I**), expressed as a percentage of controls, in the white matter of control and GCI-injected NHPs. Scale bar = 40 μm. (**J–L**) Illustrative images (**J**) and quantification (**K** and **L**) of myelin immunostaining measured by optical density; $P = 0.0140$, $t = 4.004$ (**K**) and surface threshold; $P = 0.0036$, $t = 6.572$ (**L**), expressed as a percentage of controls, in the striatum of control and GCI-injected NHPs. Scale bar = 5 mm. The horizontal line indicates the average value per group ± SD. Each dot represents one monkey of the control (black) and GCI-injected baboon monkeys (green). Comparisons were made using an unpaired *t*-test. *$P < 0.05$ compared to control animals. (**M**) Representative images (*left*) and quantification (*right*) of TPPP/p25α immunoblotting in the rostral putamen of control and GCI-injected NHPs; $P = 0.0648$, $t = 2.075$. (**N**) Representative images (*left*) and quantification (*right*) of TPPP/p25α immunoblotting in the rostral caudate nucleus of control and GCI-injected NHPs; $P = 0.2264$, $t = 0.8607$. Each dot represents one NHP of the control (black) and GCI-injected NHPs (green). Bootstrapped mean difference with 95% CI (error bar) is shown on the *right* side of each graph. Comparisons were made using an unpaired *t*-test. *$P < 0.05$ compared to control animals. CTRL = control.

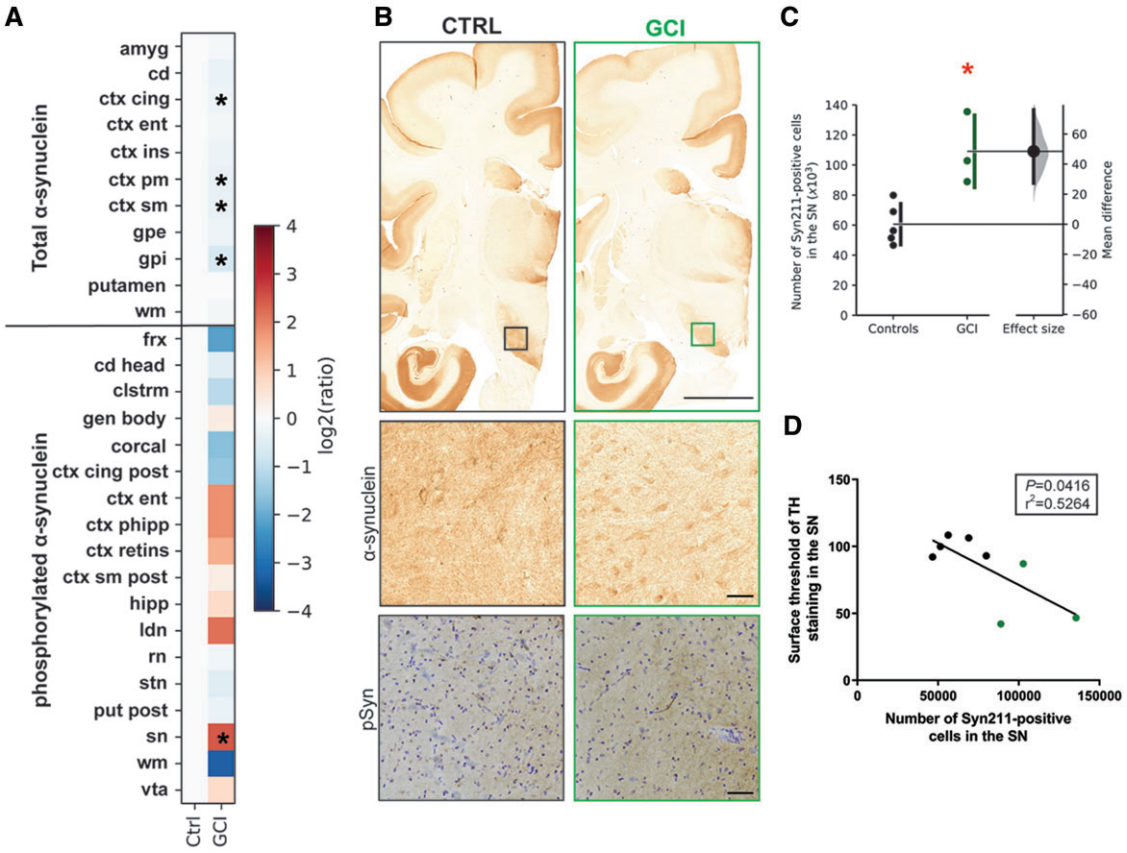

Figure 4 Intrastriatal injection of GCI-derived fractions induces a specific pattern of S129 phosphorylated α-syn levels in the NHP brain and a specific accumulation of total α-syn in the NHP substantia nigra. (**A**) Heat map representing the surface threshold of α-syn (Syn211) and S129 phosphorylated α-syn (Elan) immunostaining intensity in the brain of control and GCI-injected NHPs. The heat maps show all brain regions measured. From top to bottom, for total α-syn: amygdala (amyg), caudate nucleus (cd), cingulate cortex (ctx cing), entorhinal cortex (ctx ent), insular cortex (ctx ins), premotor cortex (ctx pm), sensorimotor cortex (ctx sm), external globus pallidus (gpe), internal globus pallidus (gpi), putamen, white matter (wm). From *top* to *bottom* for phosphorylated α-syn: fornix (frx), head of the caudate nucleus (cd head), claustrum (clstrm), geniculate body (gen body), corpus callosum (corcal), posterior cingulate cortex (ctx cing post), entorhinal cortex (ctx ent), parahippocampal cortex (ctx phipp), retroinsular cortex (ctx retins), posterior sensorimotor cortex (ctx sm post), hippocampus (hipp), lateral dorsal nucleus (ldn), red nucleus (rn), subthalamic nucleus (stn), posterior putamen (put post), substantia nigra (sn), white matter (wm), ventral tegmental area (vta). The colour bars represent the log2 value of the ratio of each brain region. (**B**) Representative coronal brain sections of endogenous α-syn immunostaining (*top*) and illustrative photomicrographs of endogenous (*middle inset*) and phosphorylated (*bottom inset*) α-syn in the SNpc of control and GCI-injected NHPs. Scale bars = 5 mm (*top*) and 50 μm (*insets*). (**C**) Scatter plot of the number of α-syn-positive cells in the substantia nigra in control and GCI-injected NHPs; $P = 0.0048$, $t = 3.746$. The horizontal line indicates the average value per group ± SD. Each dot represents one NHP of the control (black), GCI-injected NHPs (green). Comparisons were made using an unpaired *t*-test. *$P < 0.05$ compared to control animals. (**D**) Linear regression between surface threshold value of TH immunostaining and the number of α-syn-positive cells in the susbtantia nigra; $F = 6.669$, $P = 0.0416$, $r^2 = 0.5264$ for control or GCI-injected NHPs. Each dot represents one monkey of the control (black) and GCI-injected NHPs (green). Bootstrapped mean difference with 95% CI (error bar) is shown on the *right* side of each graph. Comparisons were made using an unpaired *t*-test. *$P < 0.05$ compared to control animals. CTRL = control.

GCI-injected monkeys present an MSA-like oligodendroglial loss and demyelination but only modest neuroinflammation.

GCI-containing fractions induce synuclein pathology in non-human primates

To evaluate if GCI-induced neurodegeneration and oligodendrogliopathy were associated with synuclein pathology, we quantified the levels of α-syn staining in 29 different regions of the basal ganglia and cortex (Fig. 4A and Supplementary Figs 5 and 6). While total

α-syn accumulation was modestly affected in the investigated regions (Fig. 4A, top and Supplementary Fig. 5), α-syn phosphorylated at S129 (pSyn—a pathogenic form)[45] accumulated differently in GCI-injected baboons compared to controls (Fig. 4A, bottom and B, bottom inset, and Supplementary Fig. 6). However, when looking more closely at α-syn signal in the substantia nigra, we observed a relocalization from a diffuse staining (typical of the physiological presynaptic localization of the protein) to a cellular-like staining in soma, represented by a significant increase (~50% effect size) in α-syn-positive cells (Fig. 4B and C). Of interest, the number of nigral α-syn-positive cells significantly and negatively correlated with TH-positive cell surface staining in the substantia nigra, indicating that the decrease in TH-positive cells is associated with an increase in the number of α-syn-positive cells in the substantia nigra (Fig. 4D). Biochemical investigations corroborated an increase of pSyn in the putamen and caudate nucleus in GCI-injected monkeys (Fig. 5A and B). Furthermore, using sequential extraction of Triton-X-soluble and -insoluble α-syn,[34] we detected higher levels of Triton-X-insoluble monomeric and high molecular weight forms of total α-syn (Fig. 6A and B) and pSyn (Fig. 6C and D) in the putamen, but not the caudate nucleus. Triton-X-soluble fractions were also enriched in high molecular weight forms of α-syn in the putamen (Supplementary Fig. 7A and B). Concerning pSyn, monomeric forms were enriched in both the putamen and caudate nucleus, whereas high molecular weight forms were only increased

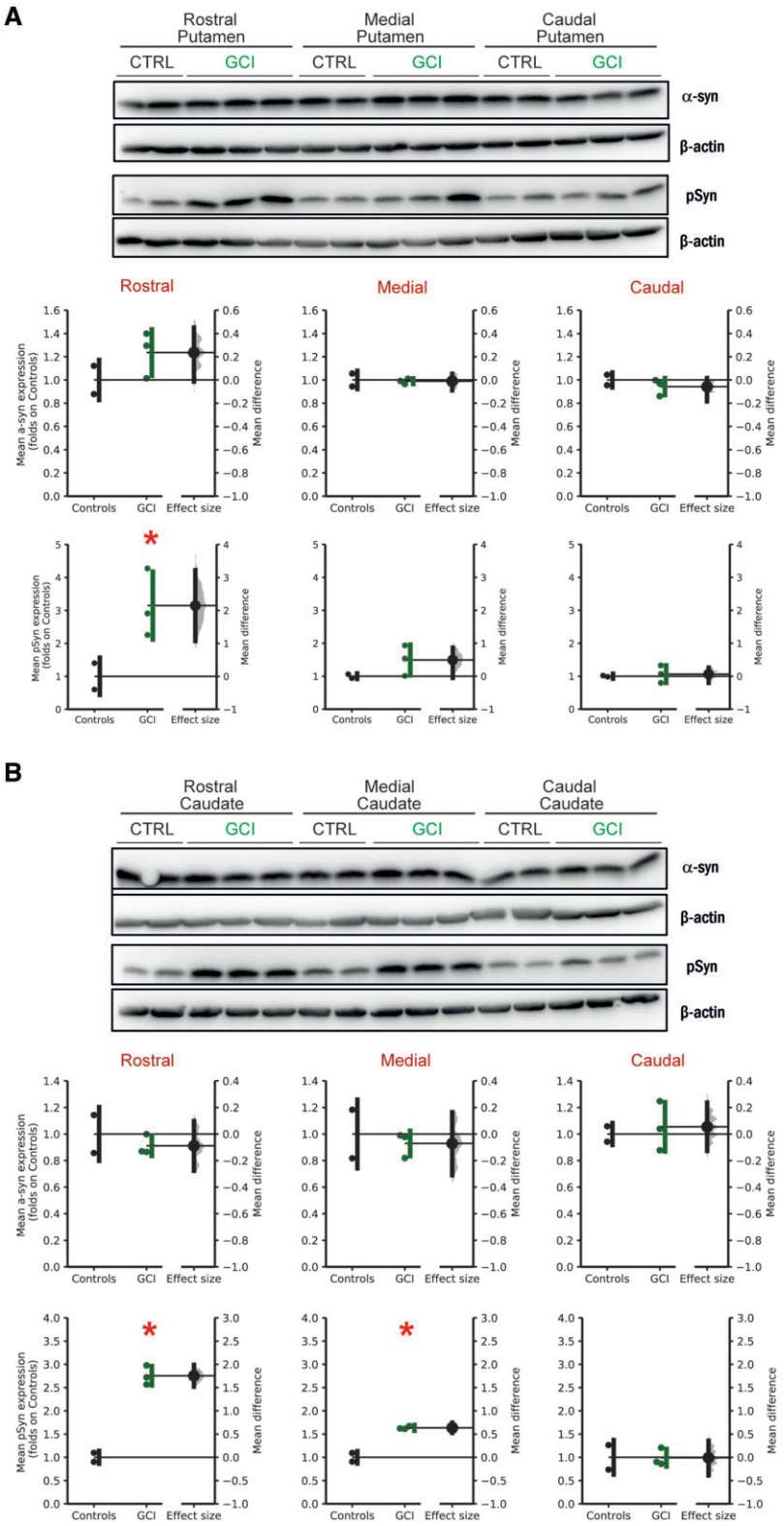

Figure 5 Total protein extracts of putamen and caudate nucleus reveal an accumulation of S129-phosphorylated α-syn after GCI injections. (**A**) Representative images (*top*) and quantification (*bottom*) of total protein extracts of α-syn and S129-phosphorylated α-syn (pSyn) immunoblotting using Syn1 and EP1536Y antibodies in the rostral, medial and caudal putamen (respectively, PuR, PuM, PuC) of control and GCI-injected NHPs (pSyn PuR: $P = 0.0040$, $t = 2607$; pSyn PuM: $P = 0.1263$, $t = 1.413$; pSyn PuC: $P = 0.3830$, $t = 0.3258$; α-syn PuR: $P = 0.1336$, $t = 1.359$; α-syn PuM: $P = 0.4120$, $t = 0.2426$; α-syn PuC: $P = 0.2169$, $t = 0.9016$). (**B**) Representative images (*top*) and quantification (*bottom*) of total protein extracts of α-syn and S129-phosphorylated α-syn (pSyn) immunoblotting using Syn1 and EP1536Y antibodies in the rostral, medial and caudal caudate nucleus (respectively, CdR, CdM, CdC) of control and GCI-injected NHPs (pSyn CdR: $P = 0.0010$, $t = 10.27$; pSyn CdM: $P = 0.0016$, $t = 8.663$; pSyn CdC: $P = 0.4845$, $t = 0.0422$; α-syn CdR: $P = 0.2579$, $t = 0.7345$; α-syn CdM: $P = 0.3378$, $t = 0.4618$; α-syn CdC: $P = 0.3660$, $t = 0.3759$). The horizontal line indicates the average value per group ± SD. Each dot represents one monkey of the control (black), GCI-injected NHPs (green). Bootstrapped mean difference with 95% CI (error bar) is shown on the *right* side of each graph. Comparisons were made using unpaired *t*-test. *$P < 0.05$ compared to control animals. CTRL = control.

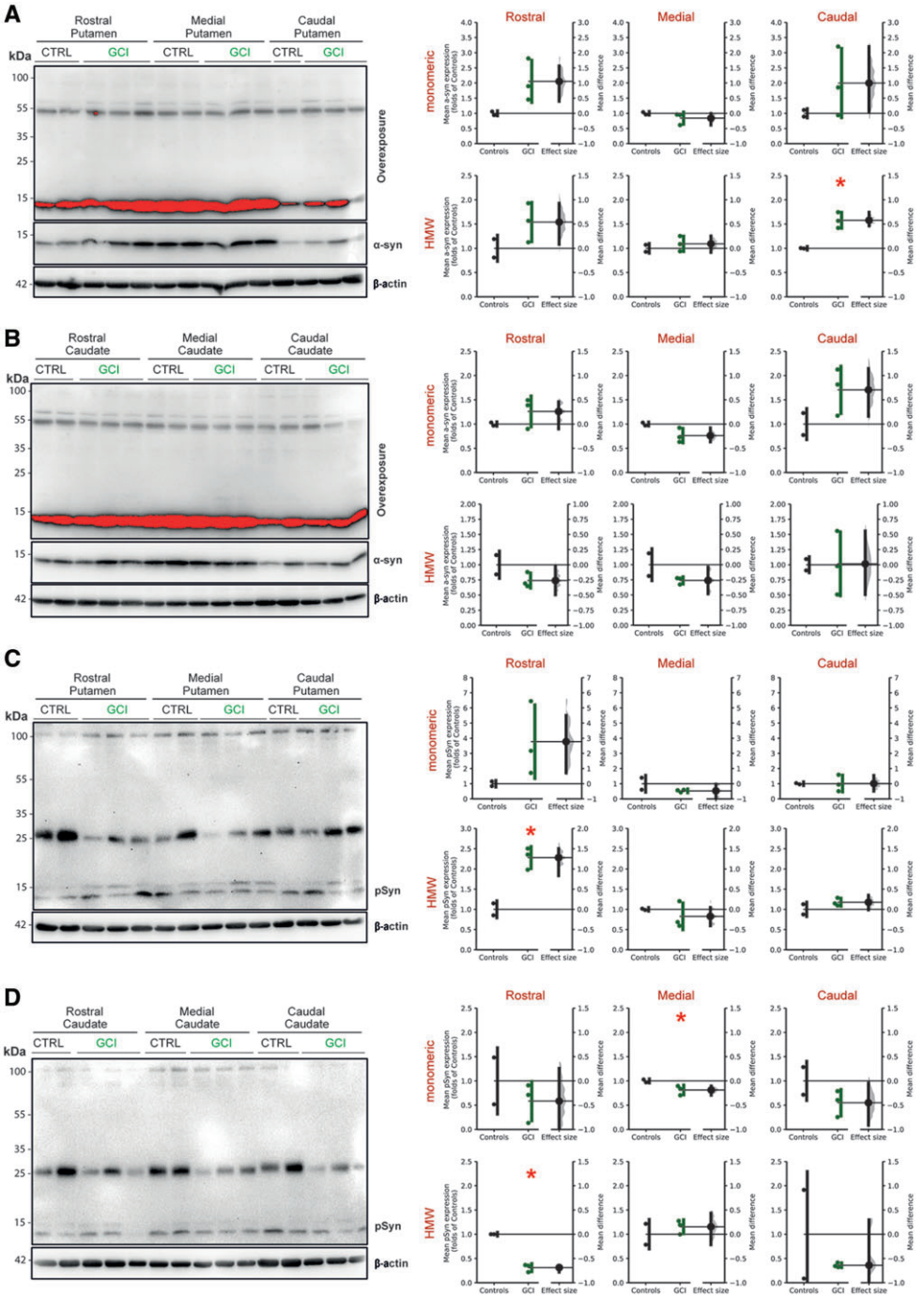

Figure 6 Subcellular fractionation of putamen and caudate nucleus reveals an accumulation of triton insoluble forms of total and S129-phosphorylated α-syn after GCI injections. (**A**) Representative images (*left*) and quantification (*right*) of Triton-X-insoluble monomeric and high molecular weight α-syn immunoblotting using Syn211 antibody in the rostral, medial and caudal putamen of control and GCI-injected baboon monkeys (14 kDa α-syn PuR: $P = 0.0675$, $t = 2.032$; 14 kDa α-syn PuM: $P = 0.1816$, $t = 1.069$; 14 kDa α-syn PuC: $P = 0.2444$, $t = 1.17$; 55 kDa α-syn PuR: $P = 0.1010$, $t = 1.628$; 55 kDa α-syn PuM: $P = 0.2606$, $t = 0.7242$; 55 kDa α-syn PuC: $P = 0.0088$, $t = 4.769$). (**B**) Representative images (*left*) and quantification (*right*) of Triton-X-insoluble monomeric and high molecular weight α-syn immunoblotting using Syn211 antibody in the rostral, medial and caudal caudate nucleus of control and GCI-injected baboon monkeys (14 kDa α-syn CdR: $P = 0.1769$, $t = 1.095$; 14 kDa α-syn CdM: $P = 0.0615$, $t = 2.13$; 14 kDa α-syn CdC: $P = 0.0882$, $t = 1.762$; 55 kDa α-syn CdR: $P = 0.0907$, $t = 1.733$; 55 kDa α-syn CdM: $P = 0.0865$, $t = 1.781$; 55 kDa α-syn CdC: $P = 0.4864$, $t = 0.03697$). (**C**) Representative images (*left*) and quantification (*right*) of Triton-X-insoluble monomeric and high molecular weight pSyn immunoblotting using EP1536Y antibody in the rostral, medial and caudal of control and GCI-injected baboon monkeys (14 kDa α-syn PuR: $P = 0.1113$, $t = 1.534$; 14 kDa α-syn PuM: $P = 0.1089$, $t = 1.555$; 14 kDa α-syn PuC: $P = 0.4868$, $t = 0.0358$; 100 kDa α-syn PuR: $P = 0.0057$, $t = 5.571$; 100 kDa α-syn PuM: $P = 0.2647$, $t = 0.7092$; 100 kDa α-syn PuC: $P = 0.1188$, $t = 1.472$). (**D**) Representative images (*left*) and quantification (*right*) of Triton-X-insoluble monomeric and high molecular weight pSyn immunoblotting using EP1536Y antibody in the rostral, medial and caudal caudate nucleus of control and GCI-injected baboon monkeys (14 kDa α-syn CdR: $P = 0.2203$, $t = 0.8865$; 14 kDa α-syn CdM: $P = 0.0456$, $t = 2.457$; 14 kDa α-syn CdC: $P = 0.1114$, $t = 1.533$; 100 kDa α-syn CdR: $P = 0.0007$, $t = 11.35$; 100 kDa α-syn CdM: $P = 0.2397$, $t = 0.8054$; 100 kDa α-syn CdC: $P = 0.2089$, $t = 0.9373$). The horizontal line indicates the average value per group ± SD. Each dot represents one monkey of the control (black), GCI-injected baboon monkeys (green). Bootstrapped mean difference with 95% CI (error bar) is shown on the *right* side of each graph. Comparisons were made using unpaired *t*-test. *$P < 0.05$ compared to control animals. CTRL = control.

in the caudate nucleus (Supplementary Fig. 7C and D). Altogether, these results indicate α-syn buildup with both a change in cellular staining and increased Triton-X-insoluble and -soluble protein expression in the striatum 2 years after GCI injection.

One of the hallmarks of MSA is the accumulation of α-syn in oligodendrocytes. We determined the cell-type specificity and distribution of α-syn expression via immunofluorescence confocal microscopy with the well-established oligodendrocyte marker CNPase and the neuronal marker NeuN. In both controls and GCI-injected monkeys, α-syn co-localized with CNPase in putaminal oligodendrocytes (Fig. 7A), with a significant increase in the number and a decrease in the size of α-syn-positive puncta in GCI-injected monkeys. This suggests that α-syn accumulates in oligodendrocytes of GCI-injected primates, with more abundant smaller puncta distributed in the oligodendrocyte. On the contrary, α-syn puncta were rare in neurons, both in controls and GCI-injected monkeys (Fig. 7B). In the remaining oligodendrocytes, co-localization of pSyn and CNPase was observed in control and GCI-injected animals, with a surprising decrease in pSyn puncta in GCI-injected baboon monkeys (Fig. 7C). In neurons, pSyn was also found in the cytoplasm of control and GCI-injected baboons (Fig. 7D). Altogether, these results suggest an accumulation of α-syn in oligodendrocytes of GCI-injected monkeys, indicating a potential first phase of MSA-related α-syn pathology induction.

Discussion

In this pilot study, we show that intracerebral injections of GCI-enriched fractions in NHPs induce most of the disease-specific aspects of MSA neuropathological features. Two years after stereotactic striatal injections, baboon monkeys inoculated with GCIs demonstrated subtle behavioural changes and neuropathological evidence of MSA pathology, including loss of both dopaminergic and striatal neurons, loss of oligodendrocytes in the putamen along with demyelination, slight neuroinflammation and accumulation of α-syn in oligodendrocytes compared to age-matched control monkeys. These observations suggest that, 2 years after injection, the GCI-exposed baboon monkeys were in an initial phase of an MSA-like condition.

Mice experiments were aimed at qualifying the GCI fractions based on dopaminergic neuron-induced toxicity. After 4 months post-injection, the supranigral injection of GCI in C57BL6/J wild-type mice led to dopamine neuron loss. Despite meeting the qualification criterion set before NHP experimentation, one may wonder why other parameters were not affected at 4 months in wild-type mice. There are few previous reports of MSA-derived extracts injected in wild-type and transgenic mice. Interestingly, a recent report showed that detergent-insoluble α-syn isolated from MSA patients could also induce neuronal inclusions in C57BL6/C3H wild-type mice at 3 months after striatal injection but failed to generate an oligodendroglial pathology.[19] Other types of extracts, i.e. brain homogenates instead of our GCI extraction procedure, have also been tested, but they were administered to transgenic α-syn-overexpressing mice. In this regard, intracerebral injections of brain extracts from MSA patients in homozygous and hemizygous TgM83 mice led to neurodegeneration and formation of α-syn-positive inclusions after 3 months.[17,18,46] Following this, another study used injections of brain homogenates from sick M83 transgenic mice or human MSA patient extracts in TgM83 mice.[47] This study demonstrated that pathological α-syn accumulation in transgenic mice was higher when inoculated with homogenates from sick M83 mice than from MSA patient extracts. Unlike our GCI inoculations, none of these injections induced neurodegeneration or synucleinopathy in wild-type mice, regardless of the inoculum.

MSA extracts have been by far less used than Parkinson's disease extracts in an experimental setting. Notably, the α-syn spreading and toxicity efficiency observed in different laboratories depends strongly on several factors, including the biochemical preparation of the inoculum, the injected quantity (in the microgram–picogram range) and volume, the choice of mouse strain, the brain areas of injection, the post-injection observational period and the potential species barrier.[17,18,46,47] Interestingly, the literature using transgenic MSA mouse models based on α-syn overexpression is more profuse and provides interesting timing considerations. The PLP-α-syn transgenic mouse model displays a loss of dopamine neurons (predominant between 2 and 4 months of age), together with age-related impairments that worsen when striatal atrophy comes into play around 10–12 months of age.[8,10,11] Besides, this model recapitulates the oligodendroglial accumulation of insoluble α-syn as well as some dysautonomic features of MSA only when mice reach 10–12 months of age.[8,48,49] Also, another recent study where preformed fibrils of α-syn were injected in both young and old wild-type C57Bl6/J mice showed the presence of oligodendroglial α-syn aggregates starting at 12–18 months.[20] Nonetheless, a recent study demonstrated the difference between the atomic structures of seeded assemblies of recombinant human α-syn fibrils compared to that of human α-syn extracts, also demonstrating the need for models using patient-derived extracts.[50] Although follow-up studies would be necessary to confirm this suggested time-related hypothesis, wild-type mice receiving GCI extracts might likely require a more extended survival period before manifesting signs of oligodendrogliopathy and demyelination in the striatum, as observed in NHPs.

One of the major unanswered questions in the field remains what triggers the localization of GCIs in oligodendrocytes compared to Lewy body formation in neurons.[51–53] Follow-up questions are whether, why, and how much α-syn accumulation in oligodendrocytes would lead to neurodegeneration, as it undoubtedly occurs in MSA patients, in α-syn transgenic mice models and in the current set of GCI-exposed NHPs. Various non-exclusive mechanisms might be at work, such as (i) the relocalization of TPPP/p25α in oligodendrocytes from the myelin sheath to the cytoplasm, which appears to be an early pathologic event that precedes α-syn aggregation[5,43]; (ii) the α-syn release from neurons to oligodendrocytes through active or passive mechanisms[54]; and (iii) non-cell autonomous factors such as pro-inflammatory or environmental factors.[55,56] In light of the ongoing debate, these cells may produce much of the protein[57–60] and the intracellular and the extracellular factors responsible for α-syn expression in oligodendrocytes. In addition, further studies are needed to determine to what extent conformational status and accumulation of α-syn and pSyn end up in oligodendrocytes. No genuine GCIs were observed in the present NHP experiments. Given the otherwise convincing reported pathology, we posit that actual formation of GCIs would take longer than the 2-year survival period imposed by the experimental design. However, redistribution of pSyn accumulation towards oligodendrocytes is present and, being concomitant to other aspects of MSA neuropathology, including TPPP/p25α accumulation,[61] we strongly suggest these animals model a pre-GCI phase. This observation raises two consequences: it suggests that MSA-derived extracts can induce oligodendroglial α-syn pathology, irrespective of the controversy on the expression of α-syn itself by oligodendrocytes. It further suggests that nigral and striatal degeneration precedes GCI formation, although linked to α-syn redistribution in oligodendrocytes. Importantly, such redistribution was not observed in NHPs injected with Lewy bodies. Taken together, this provides additional pieces to the concept of disease-related strains, which could discriminate between the occurrence of Parkinson's disease or MSA pathologies.

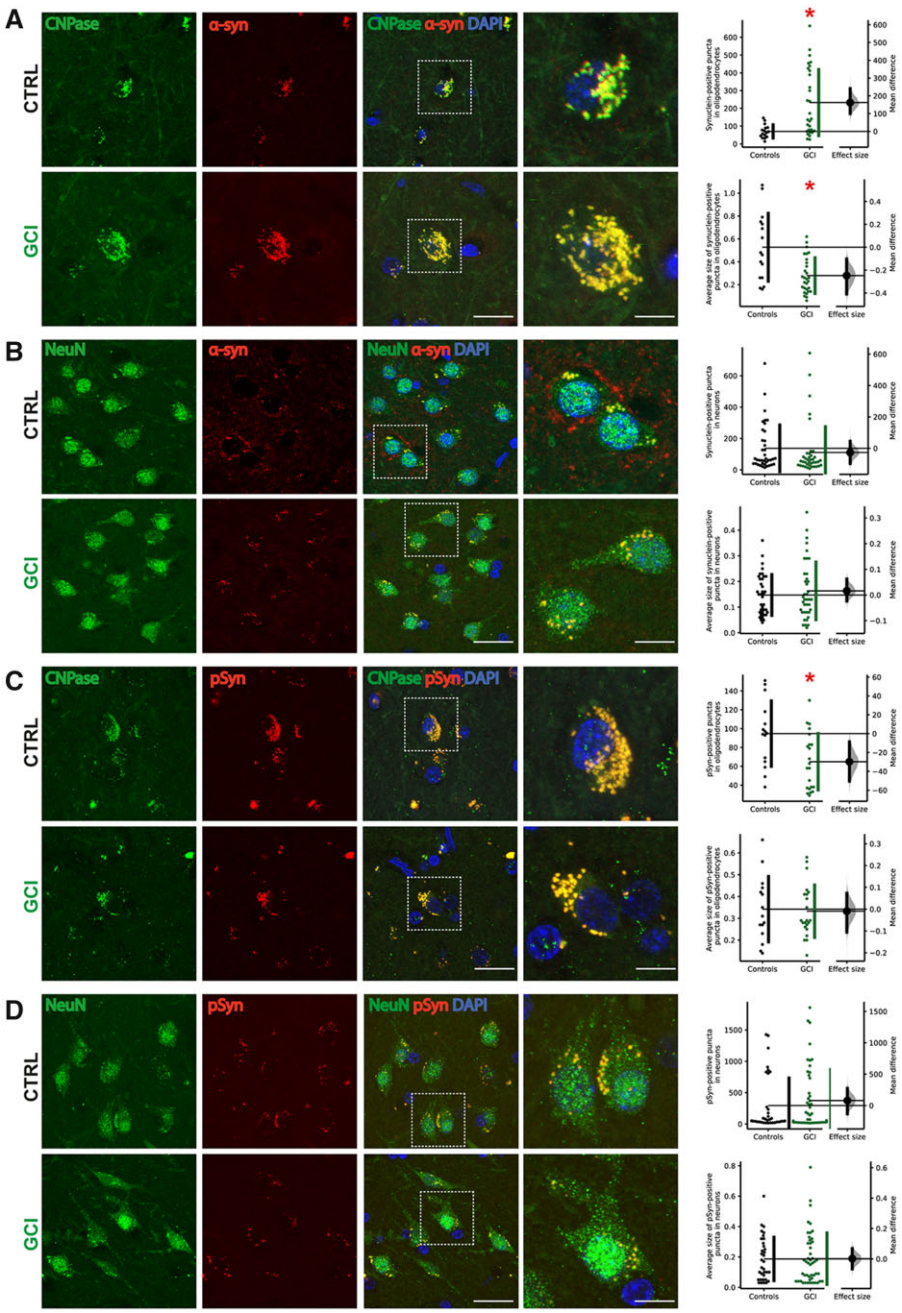

Figure 7 Injection of GCI induces co-localization of total and S129-phosphorylated α-syn in oligodendrocytes and S129-phosphorylated α-syn exclusively in NHP neurons. (**A**) Representative confocal microscopy images (*left*) and quantifications (*right*) of oligodendrocytes and α-syn immunostaining, using CNPase and MJFR1 antibodies, respectively, in the putamen of control and GCI-injected NHPs. Scale bar = 20 μm, *inset* scale bar = 10 μm. Quantifications measured puncta of α-syn staining in oligodendrocytes (*top*) $P = 0.007$, $t = 3.426$; and the average size of these puncta (*bottom*) $P = 0.003$, $t = 3.690$. (**B**) Representative confocal microscopy images (*left*) and quantifications (*right*) of neuronal and α-syn immunostaining, using NeuN and MJFR1 antibodies, respectively, in the putamen of control and GCI-injected NHPs. Scale bar = 20 μm, *inset* scale bar = 10 μm. Quantifications measured puncta of α-syn staining in neurons (*top*) $P = 0.2270$, $t = 0.7528$; and the average size of these puncta (*bottom*) $P = 0.2386$, $t = 0.7146$. (**C**) Representative confocal microscopy images (*left*) and quantification (*right*) of oligodendrocytes and phosphorylated α-syn immunostaining, using CNPase and EP1536Y antibodies, respectively, in the putamen of control and GCI-injected NHPs. Scale bar = 20 μm, *inset* scale bar = 10 μm. Quantifications measured puncta of pSyn staining in oligodendrocytes (*top*) $P = 0.0043$, $t = 2.788$; and the average size of these puncta (*bottom*) $P = 0.4757$, $t = 0.06138$. (**D**) Representative confocal microscopy images (*left*) and quantification (*right*) of neuronal and phosphorylated α-syn immunostaining, using NeuN and EP1536Y antibodies, respectively, in the putamen of control and GCI-injected NHPs. Scale bar = 20 μm, *inset* scale bar = 10 μm. Quantifications measured puncta of pSyn staining in neurons (*top*) $P = 0.2297$, $t = 0.7435$; and the average size of these puncta (*bottom*) $P = 0.4788$, $t = 0.05344$. The horizontal line indicates the average value per group ± SD. Each dot represents one cell of the control (black) or GCI-injected NHPs (green). Bootstrapped mean difference with 95% CI (error bar) is shown on the *right* side of each graph. Comparisons were made using unpaired *t*-test. *$P < 0.05$ compared to control animals. CTRL = control.

However, relying on a single snapshot at 2 years precludes a dynamic understanding of the process. It prevents us from defining whether cell death promotes accumulation of α-syn in oligodendrocytes or the contrary. What we can affirm, however, is that abnormal handling of α-syn propagates from the putamen, i.e. the location of intracerebral injection, to other brain regions, as can be seen in the heat map (Fig. 4A) with progression to cortical areas and the lateral dorsal nucleus. This suggests that GCI-induced α-syn pathology can propagate in NHPs, as shown previously for Parkinson's disease-derived α-syn species.[14–16]

While acceptable for an exploratory study, further studies would require larger NHP cohorts to reach adequate statistical power for all variables. An additional question deals with the nature of the control arm of this exploratory study. We had to predetermine the experimental groups with a known number of animals and make choices regarding the control groups at the beginning of this large-scale study. Before our experiments on olive baboons,[15,16] only two studies reported on using this species to model synucleinopathy and neurodegeneration.[62,63] We thus faced a lack of baseline parameters, for instance, references of dopaminergic-related parameters.

The present study is the MSA component of a large effort to explore the impact of Parkinson's disease and MSA patient-derived α-syn aggregates in NHPs.[15,16,21] Uninjected animals were therefore used as controls for multiple extracts, preventing the use of other several additional control individuals, in agreement with the 3R principle. This choice was further validated *a posteriori* by the discovery that, in NHPs but not in mice, a small amount of singular small Parkinson's disease-derived α-syn aggregates is as toxic as larger Parkinson's disease-derived amyloid fibrils present in the Lewy bodies.[15] Relevant to this issue, we did not inoculate animals with immunodepleted α-syn or α-syn fractions denatured with formic acid, as we previously showed that inoculation with α-syn immunodepleted fractions did induce neither neurodegeneration nor synuclein pathology.[14]

Overall, we here provide the proof-of-concept that MSA-derived GCI fractions trigger a pathogenic process in rodents and NHPs. This study widens exciting perspectives for understanding human MSA pathology *per se* and across species within the normal α-syn expression context. Further studies with more monkeys and different time points of post-mortem analysis are needed to extend our observations and appreciate the full scope of the phenotypes following GCI injections. These could also give insights into the contribution of the oligodendroglial synucleinopathy in MSA neurodegeneration to help solve the perplexing dichotomy of Parkinson's disease/DLB versus MSA.

Acknowledgements

The authors thank Carmen Lagares Martínez (Head, Veterinary Service, University of Murcia, Murcia, Spain) for administrative assistance; Maria Fermina Ros Romero and Josefa Martínez Rabadán (University of Murcia) for veterinary and husbandry support; Ana Luisa Gil, Lorena Cuenca and Ignacio Mascarell from Clinical and Experimental Neuroscience group (University of Murcia) for their technical help with various parts of the *in vivo* part of these complex experiments. We would like to thank Philippe Hantraye (MIRCen, Fontenay-aux-Roses, France) for providing a baboon stereotactic frame. The University of Bordeaux and the Centre National de la Recherche Scientifique provided infrastructural support. The samples were obtained from the Brain Bank GIE NeuroCEB (BRIF number 0033–00011), funded by the patients' associations France Alzheimer, France Parkinson, ARSEP and 'Connaître les Syndromes Cérébelleux' to which we express our gratitude.

Funding

This work was supported by a grant from the Michael J. Fox Foundation (Project Grant No. 2013–8499), Fundacion de Investigacion HM Hospitales (Madrid, Spain), the Fundación Séneca (Project Grant No: FS19540/PI/14), the TARGET PD ANR grant and The Simone and Cino Del Duca Prize from French Academy of Sciences. M.T., M.B. and M.L.A. were supported by a Ministère de l'Enseignement Supérieur et de la Recherche fellowship (France). M.B. and M.L.A. were also supported by the France Parkinson Foundation (France). This study received financial support from the French government in the framework of the University of Bordeaux's IdEx "Investments for the Future" program/GPR BRAIN_2030. The sequential α-synuclein extraction was performed in the Biochemistry and Biophysics Platform of the Bordeaux Neurocampus at the Bordeaux University funded by the LABEX BRAIN (ANR-10-LABX-43) with the help of Y. Rufin.

Competing interests

E.B. is a director and a shareholder of Motac Neuroscience Ltd. W.G.M. has served as an advisor for Lundbeck and Biohaven and has received teaching honoraria from UCB. The other authors declare no conflict of interest.

Supplementary material

Supplementary material is available at *Brain* online.

References

1. Halliday GM, Holton JL, Revesz T, Dickson DW. Neuropathology underlying clinical variability in patients with synucleinopathies. *Acta Neuropathol*. 2011;122(2):187–204.
2. McCann H, Stevens CH, Cartwright H, Halliday GM. alpha-Synucleinopathy phenotypes. *Parkinsonism Relat Disord*. 2014;20: S62–67.
3. Salvesen L, Ullerup BH, Sunay FB, et al. Changes in total cell numbers of the basal ganglia in patients with multiple system atrophy—A stereological study. *Neurobiol Dis*. 2015;74:104–113.
4. Nykjaer CH, Brudek T, Salvesen L, Pakkenberg B. Changes in the cell population in brain white matter in multiple system atrophy. *Mov Disord*. 2017;32(7):1074–1082.
5. Song YJ, Lundvig DM, Huang Y, et al. p25alpha relocalizes in oligodendroglia from myelin to cytoplasmic inclusions in multiple system atrophy. *Am J Pathol*. 2007;171(4):1291–1303.
6. Ahmed Z, Asi YT, Sailer A, et al. The neuropathology, pathophysiology and genetics of multiple system atrophy. *Neuropathol Appl Neurobiol*. 2012;38(1):4–24.
7. Recasens A, Ulusoy A, Kahle PJ, Di Monte DA, Dehay B. *In vivo* models of alpha-synuclein transmission and propagation. *Cell Tissue Res*. 2018;373(1):183–193.
8. Kahle PJ, Neumann M, Ozmen L, et al. Hyperphosphorylation and insolubility of alpha-synuclein in transgenic mouse oligodendrocytes. *EMBO Rep*. 2002;3(6):583–588.
9. Tanji K, Miki Y, Mori F, et al. A mouse model of adult-onset multiple system atrophy. *Neurobiol Dis*. 2019;127:339–349.
10. Shults CW, Rockenstein E, Crews L, et al. Neurological and neurodegenerative alterations in a transgenic mouse model expressing human alpha-synuclein under oligodendrocyte promoter: Implications for multiple system atrophy. *J Neurosci*. 2005;25(46):10689–10699.
11. Yazawa I, Giasson BI, Sasaki R, et al. Mouse model of multiple system atrophy alpha-synuclein expression in

oligodendrocytes causes glial and neuronal degeneration. *Neuron*. 2005;45(6):847–859.
12. Bassil F, Guerin PA, Dutheil N, et al. Viral-mediated oligodendroglial alpha-synuclein expression models multiple system atrophy. *Mov Disord*. 2017;32(8):1230–1239.
13. Marmion DJ, Rutkowski AA, Chatterjee D, et al. Viral-based rodent and nonhuman primate models of multiple system atrophy: Fidelity to the human disease. *Neurobiol Dis*. 2020;148:105184.
14. Recasens A, Dehay B, Bove J, et al. Lewy body extracts from Parkinson disease brains trigger alpha-synuclein pathology and neurodegeneration in mice and monkeys. *Ann Neurol*. 2014; 757(3):351–362.
15. Bourdenx M, Nioche A, Dovero S, et al. Identification of distinct pathological signatures induced by patient-derived alpha-synuclein structures in nonhuman primates. *Sci Adv*. 2020;6(20): eaaz9165.
16. Arotcarena ML, Dovero S, Prigent A, et al. Bidirectional gut-to-brain and brain-to-gut propagation of synucleinopathy in non-human primates. *Brain*. 2020;143(5):1462–1475.
17. Prusiner SB, Woerman AL, Mordes DA, et al. Evidence for alpha-synuclein prions causing multiple system atrophy in humans with Parkinsonism. *Proc Natl Acad Sci USA*. 2015;112(38): E5308–E5317.
18. Watts JC, Giles K, Oehler A, et al. Transmission of multiple system atrophy prions to transgenic mice. *Proc Natl Acad Sci USA*. 2013;110(48):19555–19560.
19. Peng C, Gathagan RJ, Covell DJ, et al. Cellular milieu imparts distinct pathological alpha-synuclein strains in alpha-synucleinopathies. *Nature*. 2018;557(7706):558–563.
20. Uemura N, Uemura MT, Lo A, et al. Slow progressive accumulation of oligodendroglial alpha-synuclein (alpha-Syn) pathology in synthetic alpha-syn fibril-induced mouse models of synucleinopathy. *J Neuropathol Exp Neurol*. 2019;78(10):877–890.
21. Teil M, Arotcarena ML, Dehay B. A new rise of non-human primate models of synucleinopathies. *Biomedicines*. 2021;9(3):272.
22. Herculano-Houzel S. Chapter 15: Neuronal scaling rules for primate brains: The primate advantage. In: Hofman MA, Falk D, eds. *Progress in brain research*. Elsevier; 2012: 325–340.
23. Herculano-Houzel S, Mota B, Wong P, Kaas JH. Connectivity-driven white matter scaling and folding in primate cerebral cortex. *Proc Natl Acad Sci*. 2010;107(44):19008–19013.
24. Carballo-Carbajal I, Laguna A, Romero-Gimenez J, et al. Brain tyrosinase overexpression implicates age-dependent neuromelanin production in Parkinson's disease pathogenesis. *Nat Commun*. 2019;10(1):973.
25. Herrero MT, Hirsch EC, Kastner A, et al. Neuromelanin accumulation with age in catecholaminergic neurons from *Macaca fascicularis* brainstem. *Dev Neurosci*. 1993;15(1):37–48.
26. Soria FN, Paviolo C, Doudnikoff E, et al. Synucleinopathy alters nanoscale organization and diffusion in the brain extracellular space through hyaluronan remodeling. *Nat Commun*. 2020;11(1): 3440.
27. Iwatsubo T, Yamaguchi H, Fujimuro M, et al. Lewy bodies: Purification from diffuse Lewy body disease brains. *Ann N Y Acad Sci*. 1996;786:195–205.
28. Dauer W, Kholodilov N, Vila M, et al. Resistance of alpha-synuclein null mice to the parkinsonian neurotoxin MPTP. *Proc Natl Acad Sci USA*. 2002;99(22):14524–14529.
29. Arotcarena M-L, Bourdenx M, Dutheil N, et al. Transcription factor EB overexpression prevents neurodegeneration in experimental synucleinopathies. *JCI Insight*. 2019;4(16):e129719.
30. Camus SM, Blois-Heulin C, Li Q, Hausberger M, Bezard E. Behavioural profiles in captive-bred cynomolgus macaques: Towards monkey models of mental disorders? *PLoS One*. 2013; 8(4):e62141.
31. Camus SM, Rochais C, Blois-Heulin C, Li Q, Hausberger M, Bezard E. Birth origin differentially affects depressive-like behaviours: Are captive-born cynomolgus monkeys more vulnerable to depression than their wild-born counterparts? *PLoS One*. 2013;8(7):e67711.
32. Camus SM, Rochais C, Blois-Heulin C, Li Q, Hausberger M, Bezard E. Depressive-like behavioral profiles in captive-bred single- and socially-housed rhesus and cynomolgus macaques: A species comparison. *Front Behav Neurosci*. 2014;8:47.
33. Crameri F, Shephard GE, Heron PJ. The misuse of colour in science communication. *Nat Commun*. 2020;11(1):5444.
34. Deffains M, Canron MH, Teil M, et al. L-DOPA regulates alpha-synuclein accumulation in experimental Parkinsonism. *Neuropathol Appl Neurobiol*. 2021;47(4):532–543.
35. de Freitas Silva DM, Ferraz VP, Ribeiro AM. Improved high-performance liquid chromatographic method for GABA and glutamate determination in regions of the rodent brain. *J Neurosci Methods*. 2009;177(2):289–293.
36. Marti M, Trapella C, Viaro R, Morari M. The nociceptin/orphanin FQ receptor antagonist J-113397 and L-DOPA additively attenuate experimental Parkinsonism through overinhibition of the nigrothalamic pathway. *J Neurosci*. 2007;27(6):1297–1307.
37. Virtanen P, Gommers R, Oliphant TE, et al.; SciPy 1.0 Contributors. SciPy 1.0: Fundamental algorithms for scientific computing in Python. *Nat Methods*. 2020;17(3):261–272.
38. van der Walt S, Colbert SC, Varoquaux G. The NumPy array: A structure for efficient numerical computation. *Comput Sci Eng*. 2011;13(2):22–30.
39. Hunter JD. Matplotlib: A 2D graphics environment. *Comput Sci Eng*. 2007;9(3):90–95.
40. Ho J, Tumkaya T, Aryal S, Choi H, Claridge-Chang A. Moving beyond *P* values: Data analysis with estimation graphics. *Nat Methods*. 2019;16(7):565–566.
41. Albin RL, Young AB, Penney JB. The functional anatomy of basal ganglia disorders. *Trends Neurosci*. 1989;12(10):366–375.
42. Mavroeidi P, Arvanitaki F, Karakitsou AK, et al. Endogenous oligodendroglial alpha-synuclein and TPPP/p25alpha orchestrate alpha-synuclein pathology in experimental multiple system atrophy models. *Acta Neuropathol*. 2019;138(3):415–441.
43. Ota K, Obayashi M, Ozaki K, et al. Relocation of p25alpha/tubulin polymerization promoting protein from the nucleus to the perinuclear cytoplasm in the oligodendroglia of sporadic and COQ2 mutant multiple system atrophy. *Acta Neuropathol Commun*. 2014;2:136.
44. Valera E, Masliah E. The neuropathology of multiple system atrophy and its therapeutic implications. *Auton Neurosci*. 2018; 211:1–6.
45. Fujiwara H, Hasegawa M, Dohmae N, et al. alpha-Synuclein is phosphorylated in synucleinopathy lesions. *Nat Cell Biol*. 2002; 4(2):160–164.
46. Woerman AL, Patel S, Kazmi SA, et al. Kinetics of alpha-synuclein prions preceding neuropathological inclusions in multiple system atrophy. *PLoS Pathog*. 2020;16(2):e1008222.
47. Sargent D, Verchere J, Lazizzera C, et al. 'Prion-like' propagation of the synucleinopathy of M83 transgenic mice depends on the mouse genotype and type of inoculum. *J Neurochem*. 2017;143(1): 126–135.
48. Fernagut PO, Meissner WG, Biran M, et al. Age-related motor dysfunction and neuropathology in a transgenic mouse model of multiple system atrophy. *Synapse*. 2014;68(3):98–106.
49. Refolo V, Bez F, Polissidis A, et al. Progressive striatonigral degeneration in a transgenic mouse model of multiple system atrophy: Translational implications for interventional therapies. *Acta Neuropathol Commun*. 2018;6(1):2.

50. Lovestam S, Schweighauser M, Matsubara T, et al. Seeded assembly *in vitro* does not replicate the structures of alpha-synuclein filaments from multiple system atrophy. *FEBS Open Bio*. 2021;11(4):999–1013.
51. Shahnawaz M, Mukherjee A, Pritzkow S, et al. Discriminating alpha-synuclein strains in Parkinson's disease and multiple system atrophy. *Nature*. 2020;578(7794):273–277.
52. Lau A, So RWL, Lau HHC, et al. alpha-Synuclein strains target distinct brain regions and cell types. *Nat Neurosci*. 2020;23(1):21–31.
53. Holec SAM, Woerman AL. Evidence of distinct alpha-synuclein strains underlying disease heterogeneity. *Acta Neuropathol*. 2020;142(1):73–86.
54. Yu Z, Shi M, Stewart T, et al. Reduced oligodendrocyte exosome secretion in multiple system atrophy involves SNARE dysfunction. *Brain*. 2020;143(6):1780–1797.
55. Stefanova N, Reindl M, Neumann M, Kahle PJ, Poewe W, Wenning GK. Microglial activation mediates neurodegeneration related to oligodendroglial alpha-synucleinopathy: Implications for multiple system atrophy. *Mov Disord*. 2007; 22(15):2196–2203.
56. Lee HJ, Suk JE, Patrick C, et al. Direct transfer of alpha-synuclein from neuron to astroglia causes inflammatory responses in synucleinopathies. *J Biol Chem*. 2010;285(12):9262–9272.
57. Miller DW, Johnson JM, Solano SM, Hollingsworth ZR, Standaert DG, Young AB. Absence of alpha-synuclein mRNA expression in normal and multiple system atrophy oligodendroglia. *J Neural Transm (Vienna)*. 2005;112(12):1613–1624.
58. Jin H, Ishikawa K, Tsunemi T, Ishiguro T, Amino T, Mizusawa H. Analyses of copy number and mRNA expression level of the alpha-synuclein gene in multiple system atrophy. *J Med Dent Sci*. 2008;55(1):145–153.
59. Asi YT, Simpson JE, Heath PR, et al. Alpha-synuclein mRNA expression in oligodendrocytes in MSA. *Glia*. 2014;62(6):964–970.
60. Djelloul M, Holmqvist S, Boza-Serrano A, et al. Alpha-synuclein expression in the oligodendrocyte lineage: An *in vitro* and *in vivo* study using rodent and human models. *Stem Cell Reports*. 2015; 5(2):174–184.
61. Papp MI, Lantos PL. The distribution of oligodendroglial inclusions in multiple system atrophy and its relevance to clinical symptomatology. *Brain*. 1994;117(2):235–243.
62. Kowall NW, Hantraye P, Brouillet E, Beal MF, McKee AC, Ferrante RJ. MPTP induces alpha-synuclein aggregation in the substantia nigra of baboons. *Neuroreport*. 2000;11(1):211–213.
63. McRitchie DA, Cartwright H, Pond SM, et al. The midbrain dopaminergic cell groups in the baboon *Papio ursinus*. *Brain Res Bull*. 1998;47(6):611–623.